Sensing and Bio-Sensing Research 1 (2014) 34–40

Contents lists available at ScienceDirect

Sensing and Bio-Sensing Research

journal homepage: www.elsevier.com/locate/sbsr

Fabrication and characterization of gas sensor micro-arrays

H. Shokry Hassan [a,*], A.B. Kashyout [a], I. Morsi [b], A.A.A. Nasser [b], A. Raafat [b]

[a] Electronic Materials Researches Department, Advanced Technology and New Materials Researches Institute, City of Scientific Researches and Technological Applications, New Borg El-Arab City, Alexandria 21934, Egypt
[b] Arab Academy for Science and Technology, and Maritime Transport, Alexandria 21936, Egypt

ARTICLE INFO

Keywords:
Sol–gel method
Quadrature gas sensor
Nanostructures
Doping ratios

ABSTRACT

A novel structures of nanomaterials gas sensors array constructed using ZnO, and ZnO doped with Al via sol–gel technique. Two structure arrays are developed; the first one is a double sensor array based on doping with percentages of 1% and 5%. The second is a quadrature sensor array based on several doping ratios concentrations (0%, 1%, 5% and 10%). The morphological structures of prepared ZnO were revealed using scanning electron microscope (SEM). X-ray diffraction (XRD) patterns reveal a highly crystallized wurtzite structure and used for identifying phase structure and chemical state of both ZnO and ZnO doped with Al under different preparation conditions and different doping ratios. Chemical composition of Al-doped ZnO nanopowders was performed using energy dispersive X-ray (EDS) analysis. The electrical characteristics of the sensor are determined by measuring the two terminal sensor's output resistance for O_2, H_2 and CO_2 gases as a function of temperature.

1. Introduction

Nowadays, there is a great interest in implementing sensing devices in order to improve environmental and safety control of gases [1]. There is also a great need of this kind of sensors to carry out the optimization of combustion reactions in the emerging transport industry and in domestic and industrial applications [2]. It has been known for a long time that, the adsorption of gas molecules on a metal-oxide semiconductor surface can cause a significant change in the electrical resistance of the material [3].

Nanostructured materials have attracted extreme attention due to their novel properties that are strongly depended on the size, specific surface area, and morphology [4,5]. In particular, ZnO, as one of the most important semiconductors, has attracted much interest due to its unique material properties, such as wide band gap (3.37 eV), big excitation binding energy (60 meV), and large piezoelectricity constant [6,7]. Therefore, ZnO-based nanomaterials have been widely used in electronics, optoelectronics, sensors, photocatalysis, and biomedical sciences [8–11].

As the present research results on all kinds of semiconductor metal oxides have shown, ZnO may be one of the most hopeful candidates due to its mature fabrication technology, which can produce all kinds of ZnO nanostructures, such as nanowires, nanorods, nanobelts [12], nanoribbons, etc.

It is well known that the sensing performance of the gas sensors can be enhanced by adjustment of the microstructure, doping of dopant or using a small amount of noble catalyst, etc. [13–17]. Although it is proved that the nanocrystalline ZnO is one of the most promising metal oxides for gas sensors due to the unique conductance characteristics and large surface to volume ratio, their sensing performances can also be improved dramatically by the synergistic effects of the catalyst or dopant on the pure nanocrystalline ZnO.

Even though many ZnO-based gas sensing elements with high specific surface areas have been investigated and reported [18], and some of their grain sizes are as low as a few tens of nanometers, their gas sensitivities deriving from these ZnO nanomaterials have not been greatly enhanced as yet. The reasons for this phenomenon have not been discussed systematically up to now.

The sol–gel process is defined generally as: the process that involves the transition of a system from a liquid "sol" (mostly colloidal) into a solid "gel" phase [19]. Hydrolysis, condensation and drying are tree key steps in determining the properties of the final product in sol–gel processing. Sol–gel processes have several advantages over other techniques for synthesizing nanopowders of metal oxides. These include the production of ultrafine porous powders and homogeneity of the product as a result of homogenous mixing of the starting materials on the molecular level. Also, sol–gel processing holds strong promise for employment industrially on

* Corresponding author. Tel.: +20 1282305425; fax: +20 3 4593414.
E-mail addresses: hassan.shokry@gmail.com (H. Shokry Hassan), hady8@yahoo.com (A.B. Kashyout), drimanmorsi@yahoo.com (I. Morsi), menem_1954@yahoo.com (A.A.A. Nasser), amira.raafat308@gmail.com (A. Raafat).

http://dx.doi.org/10.1016/j.sbsr.2014.04.001
2214-1804/

large scales [20]. In this work we have chosen the sol–gel technique for the previous advantages.

In this work, sol–gel route was used to prepare ZnO and ZnO:Al nanomaterials. Different Al doping ratios were incorporated into the ZnO matrix and their effects on the morphological structures of the prepared nanopowders and properties of gas sensing were also studied. Two different array structures were designed and prepared from undoped and doped ZnO to be utilized as a gas sensor array for different kinds of gases as a function of temperature.

2. Materials and methods

2.1. Preparation of ZnO and ZnO:Al nanopowders and films fabrication

The ZnO nanopowders were investigated using sol–gel technique by mixing 6 ml of 1 M zinc acetate aqueous solution and a 6 ml of 10 M NaOH aqueous solution and added into 15 ml alcohol and 1 ml of triethanolamine (TEA). Then the mixture was stirred at room temperature in a glass beaker under magnetic stirring for 30 min. In case of preparing 1, 5 and 10 wt% Al-doped ZnO; an equivalent amount of aluminum chloride is added to the mixture zinc acetate dehydrate, alcohol and TEA then stirred for 30 min. The resulting solutions were aged at 70 °C for 60 min. The final obtained white powders were filtered and washed several times with alcohol and distilled water to remove any residual salts, centrifuged at 6000 rpm for 30 min, and then dried at 60 °C under air atmosphere.

2.2. Preparation and Characterization of solid state semiconductor gas sensor array

Different colloidal suspensions were obtained by mixing the synthesized ZnO nanopowders either doped with various doping ratios or un-doped with ethanol and stirring the resulting suspension overnight. Ethanolic solution with ZnO content of about 20% by weight was attended. The glass substrates is ultrasonically cleaned in acetone for 15 min, and then rinsed several times with demonized water and ethanol. The heater (platinum heater) was deposited onto the previously cleaned glass substrate by sputtering machine (Turbo Sputtering RF & DC Power Supplies Deposition System Model Hummer 8.1) (P = 100 W RF, t = 5 min). Then the suspension of ZnO was applied by a wafer spinner machine (100 rpm, 2 min) (Model Polos 300 AWS). The film was then allowed to dry in air. ZnO films were sintered shortly after deposition in air flow at 400 °C for 5 min.

The copper masks shown in Fig. 1(a) and (b) were placed over prepared ZnO films to gain double or quadrature gas sensor array. Finally, Pt contact electrodes were deposited on doped and un-doped ZnO films using a sputtering machine (P = 100 W RF, t = 5 min).

All tested gases (O_2, H_2 and CO_2) were passed inside the homemade gas chamber through opening the chamber valve. The resistivity of the gas sensor device was evaluated and the resultant sensitivity was plotted as a function of gas temperature for all gases. The sensor response for different sensor arrays (double or Quadrature

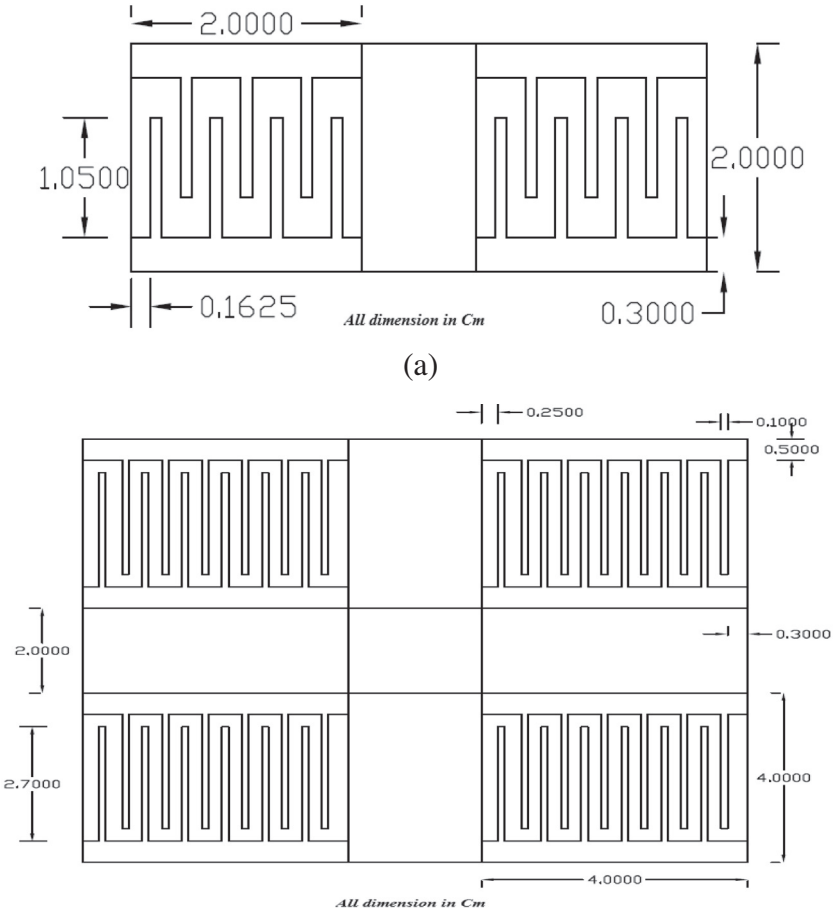

Fig. 1. (a) Mask of double sensor array, (b) Mask of Quadrature sensor array.

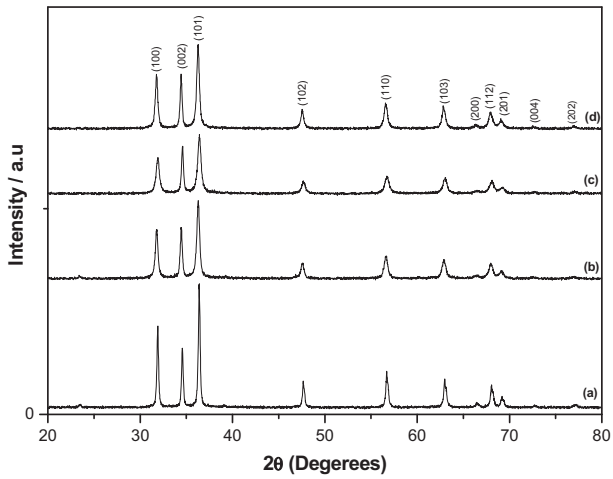

Fig. 2. XRD pattern of nanoparticles: (a) pure ZnO, (b) ZnO:Al = 99:1, (c) ZnO:Al = 95:5, (d) ZnO:Al = 9:1.

array) was defined as the ratio ($S = R_a/R_g$) of the resistance of the sensor in dry air (R_a) to that in target gases (R_g) at each temperature.

2.3. Characterization of ZnO and Al-doped ZnO nanopowders

The physical properties of the prepared ZnO nanopowder either doped or un-doped and their corresponding thick films were characterized using different techniques. X-ray diffraction patterns of the nanopowders were obtained using Schimadzu 7000 Diffractometer operating with Cu $K\alpha_1$ radiation ($\lambda = 0.15406$ nm) generated at 30 kV and 30 mA with scan rate of 2° min^{-1} for 2θ values between 20° and 80°. ZnO:Al nanopowders used for the realization of gas sensor device (ZnO film, heater and two Pt electrodes) were investigated by scanning electron microscopy (SEM) (JEOL JSM 6360LA, Japan). Chemical composition of the Al-doped ZnO nanoparticles was performed with energy dispersive X-ray analysis (EDS).

3. Results and discussion

In order to attain different morphological nanostructures from the synthesized zinc oxide, the preparation conditions of zinc oxide have been varied. The variation impact of these synthesis parameters on the physical properties of the prepared zinc oxide powder are examined for optimizing the nanorod formation.

3.1. Effect of Al doping process on ZnO characteristics

1 M Zn $(CH_3COO)_2{\cdot}2H_2O$ in presence of 1 ml of tri-ethanol amine (TEA) and 6 ml of 10 M NaOH aqueous solution and adjusting pH value of the agitated reaction mixture at 10 using ammonia solution and a mixing speed of 100 rpm under heating at 70 °C for 24 h is prepared. These preparation parameters are indicated as the best conditions for producing ZnO nanorods with highest

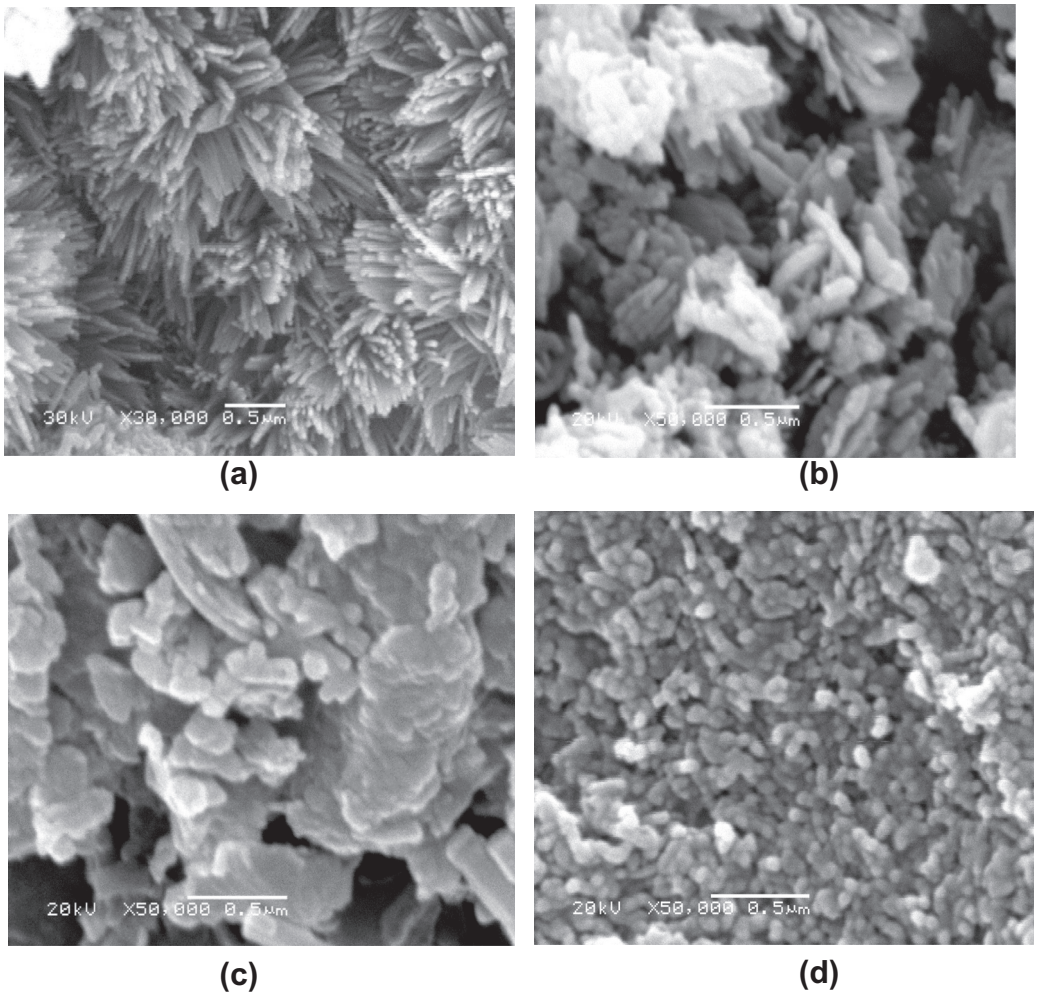

Fig. 3. SEM micrographs of (a) pure ZnO, (b) ZnO:Al = 99:1, (c) ZnO:Al = 95:5, (d) ZnO:Al = 9:1.

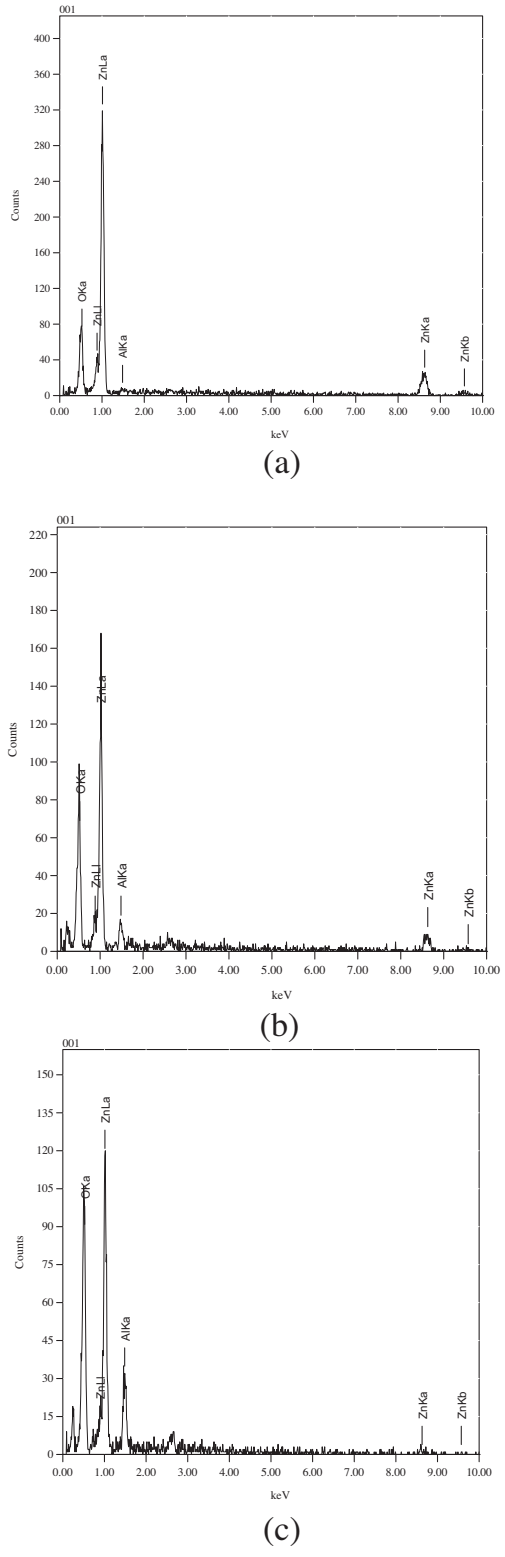

Fig. 4. EDS Spectra of ZnO doped with (a) 1 wt%, (b) 5 wt% and (c) 10 wt% Al.

degree of crystallinity. It is used to determine the effect of different dopant weight ratios to produce dopant ZnO nanoparticles.

3.1.1. X-ray diffraction analysis

All the diffraction peaks are indexed to be those of hexagonal wurtzite ZnO as shown in Fig. 2 which agrees well with those given in relevant XRD database (JCPDS card No. 01-089-1397). No characteristic peaks of other impurities are observed, which indicates that Al^{3+} is incorporated in zinc oxide matrix via substituting Zn^{2+}. Besides, there exists a minor difference in the pattern and intensity of the (100), (002) and (101) peaks of various Al doped ZO nanopowder samples with different concentrations of Al dopant (Fig. 2(b)–(d)), which implies that the effect of Al dopant on the crystal structure, and grain size of as-synthesized ZnO/Al nanostructures is concentration-dependent [21].

3.1.2. Morphological structure (SEM)

Fig. 3 shows the SEM images of pure ZnO, ZnO doped with 1%, 5%, and 10% Al respectively. That aluminum presence in any ratio changes the morphological structure from a uniform nonorods to nanoparticles. It is clear that, the ZnO nanostructures depended on the doping ratio. For pure ZnO, well-formed nanorods structures with average length of 1μm and a diameter of 100 nm have been predominated Fig. 3(a). With starting doping process with Al doping ratio 1%, ZnO nanorods come to be shorter in length and the diameters increase as shown in Fig. 2(b). Increasing in doping ratio of Al to be 5% leads to the ZnO nanorods convert to elongated nanoparticles, then to spherical nanoparticles with 10% Al doping ratio respectively Fig. 3(b) and (c). It implies that Al have an important effect on the crystallization and growth of ZnO nanoparticles [22].

3.1.3. Energy dispersive X-ray (EDS) analyses

Fig. 4 shows the energy dispersive X-ray analysis (EDS) of ZnO nanopowder doped with 1, 5, 10 wt% Al. According to Table 1, Al weight ratio in nanopowders as detected by (EDS) analysis is 1.19%, which is in accordance with the starting Al amount in the solution (1%).

The weight ratio resulted in the starting weight ratio of Al (5%) is 4.95% as shown in Table 2. Table 3 shows EDS of ZnO nanopowders doped with 10 wt% of Al which resulted in 9.91%. All results are indicating to the actual starting Sb element.

3.2. Gas sensitivity of the thick films as a function of temperature

3.2.1. Gas sensors structures

There are two arrays structures have been developed as the following:

Table 1
The EDS analysis of ZnO doped with 1 wt% Al.

Element	(keV)	Mass%	Error%	At%	*K*
O	0.525	37.97	0.31	70.62	42.0203
Al	1.486	1.19	0.48	1.54	0.5074
Zn	8.630	60.84	1.93	27.84	57.4723
Total		100.00		100.00	

Table 2
The EDS analysis of ZnO doped with 5 wt% Al.

Element	(keV)	Mass%	Error%	At%	*K*
O	0.525	40.42	0.71	71.25	46.1693
Al	1.486	4.95	1.07	5.18	1.9278
Zn	8.630	54.63	4.53	23.57	51.9029
Total		100.00		100.00	

Table 3
The EDS analysis of ZnO doped with 10 wt% Al.

Element	(keV)	Mass%	Error%	At%	*K*
O	0.525	71.89	0.45	84.47	46.1693
Al	1.486	18.20	0.60	12.68	1.9278
Zn	8.630	9.91	4.17	2.85	51.9029
Total		100.00		100.00	

The first array structure is double sensor array, which has been designed with two different ways:

(A) Both of ZnO:Al = 99:1 and 95:5 together at the same cell.
(B) Both pure ZnO and ZnO:Al = 9:1 together at the same cell as shown in Fig. 5(a) and (b).

The second array structure is quadrature sensor array which using pure ZnO, 1%, 5% and 10% Al doping element as shown in Fig. 6. This structure is consists of four sensors with different amount of doping at the same cell. The behavior of each gas sensor array structure has been studied for three kinds of gases (H_2, O_2 and CO_2 gas).

3.2.2. Gas sensing performance of the fabricated gas sensor devices

Solid state gas sensor consists of four main components, isolated substrate (glass, ceramics, etc.), heater, semiconductor metal oxide, and two electrodes was fabricated as semiconductor gas sensor (SGS) and tested for the same different concentration (100 ppm) of gases. Furthermore, different doped ZnO samples were applied as gas devices to determine the optimum dopant element and its proper doping weight ratios for high gas sensitivity. The gas response "*S*" is given by [23]

$$S = \frac{R_a}{R_g} \times 100 \quad (1)$$

where R_a and R_g express the resistance of the sensor in air and in detecting gas, respectively. The effect of the temperature on gas sensitivity of the fabricated devices for the several studied analytic gases was measured as a function of their electrical resistance.

Figs. 7–9 present the gas sensitivities as a function of operating temperature, for all investigated samples. For O_2 gas, it can be observed, from the respective dependences that, the sensitivity increases with increasing working temperature, reach a maximum value (from 100 to 120 °C, which considered low working temperature) and then falls with further increase in operating temperature. Also, it is clear that, the quadrature gas sensor array provides higher sensitivity than the double gas sensor array since, the maximum sensitivity for double gas sensor array is about 70% but for quadrature gas sensor array the maximum sensitivity reached to more than 90%. For H_2 gas, it is observed that, the maximum sensitivity for double gas sensor array is about 90% and the maximum quadrature gas sensor array's sensitivity accomplished more than 98% as shown in Fig. 8. CO_2 double gas sensor array present the lowest gas sensitivity, which attained to 48%, while the quadrature gas sensor array, the maximum sensitivity reached to 94%.

The gas sensing mechanism is based on the surface reactions between adsorbed oxygen and tested gas. It is already known that atmospheric oxygen molecules are adsorbed on the surface of n-type semiconductor oxides in the forms of O^- and O^{2-} and it deplete electrons from the conduction band [24,25]. When the tested molecules react with negatively charged oxygen, the trapped electrons are given back to conduction band of investigated films. It is supposed that the energy released during decomposition of adsorbed ammonia molecules is sufficient such that the electrons to jump up into the conduction of films, causing an increase in the conductivity of the sensor. By increasing the operating temperature, the thermal energy will increase so as to stimulate the oxidation of the tested gases (O_2, H_2 and CO_2). The reducing gas (H_2) donates electrons to the investigated gas sensor films; therefore the resistance decreases [26]. The point at which the gas sensitivity reaches maximum is the thermal energy needed for the reaction to proceed. At higher operating temperatures the gas sensitivity decreases, because of the oxygen molecules, which are desorbed from the surface of the sensor [27].

Instead, for Al:ZnO films, the sensitivity values increase, by comparison with pure ZnO. For investigated films, an increase of sensitivity with the increase of Al concentration in ZnO host is observed.

In fact, doping is a way to influence not only the structural properties such as grains shape, size and surface morphology, etc. but also the electrical properties. It was reported before that, gas sensing improved properties are achieved in the case of doped materials, mixed materials, etc. [28]. The improvement of gas sensing properties was mainly attributed to the increase of oxygen vacancies-related surface defects, which provided more effective sites for reaction [29,30]. The suggested mechanism for O_2 gas sensing as the following [31]:

$$O_{2(gas)} \rightarrow O_{2(ads)} \quad (2)$$

$$O_{2(ads)} + e^- \rightarrow O^-_{2(ads)} \quad (3)$$

$$O^-_{2(ads)} + e^- \rightarrow 2O^-_{(ads)} \quad (4)$$

$$2O^-_{(ads)} + e^- \rightarrow O^{2-}_{(ads)} \quad (5)$$

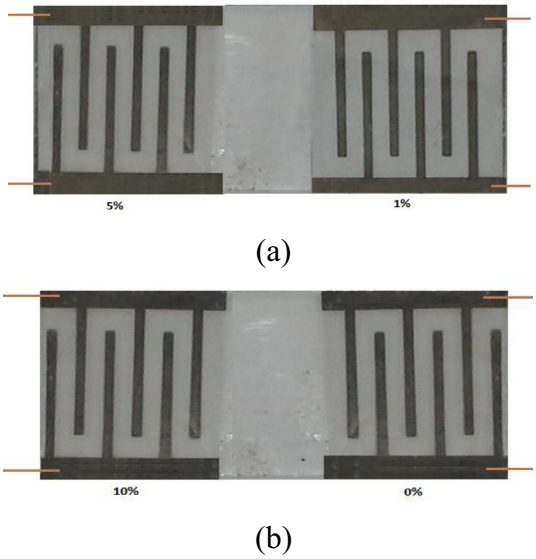

Fig. 5. Double ZnO gas sensor array (a) 1%, 5% Al doping ratio, (b) pure and 10% Al doping ratio.

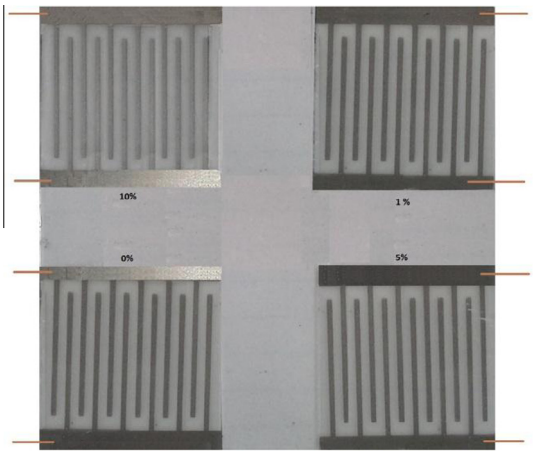

Fig. 6. Quadrature gas sensor array.

In these surface reactions, (gas) and (ads) stands for free gas and species adsorbed on the surface respectively, e^- stands for electrons contributed by ZnO. $O^-_{2(ads)}$, $O^-_{(ads)}$ and $O^{2-}_{(ads)}$ stand for the different physisorbed and chemisorbed surface oxygen species. Reactions (3)–(5) are known to be triggered in turn at increasing temperatures: the $O^-_{2(ads)}$ is the major oxygen species below 150 °C and $O^{2-}_{(ads)}$ becomes dominant when the temperature is above 450 °C; while when the temperature is in the range of 150 °C to 450 °C, $O^-_{(ads)}$ plays the major role which represent our case study [32].

For the reducing gas (H_2), adsorbs at the sensor surface and reacts with chemisorbed oxygen species, and, in particular, with

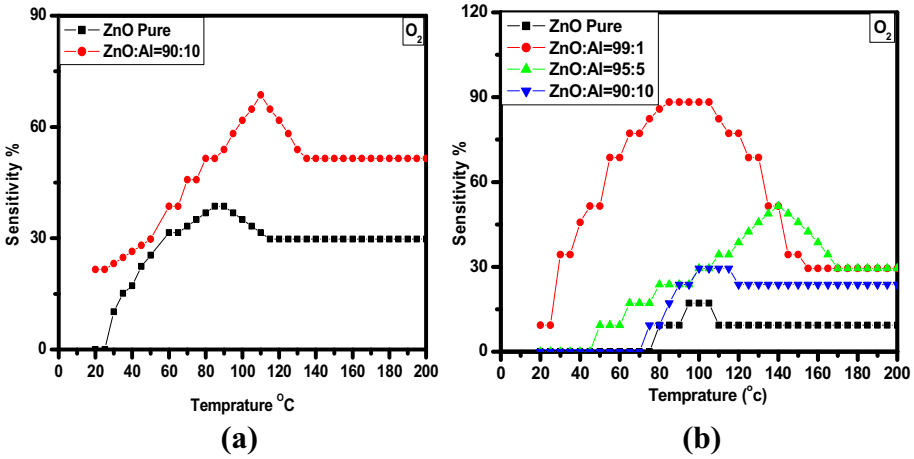

Fig. 7. Response of (a) double ZnO gas sensor, (b) quadrature pure ZnO and 1%, 5%, and 10% Al-doped ZnO gas sensors measured as a function of temperature for O_2 gas.

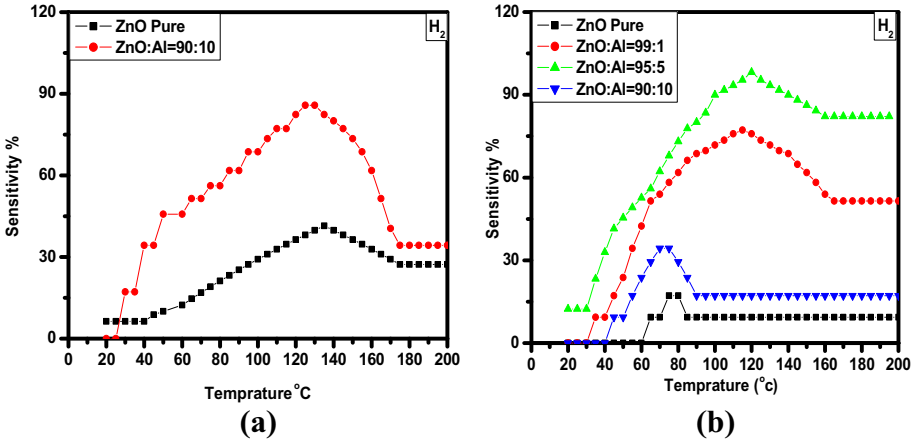

Fig. 8. Response of (a) double ZnO gas sensor, (b) quadrature pure ZnO and 1%, 5%, and 10% Al-doped ZnO gas sensors measured as a function of temperature for H_2 gas.

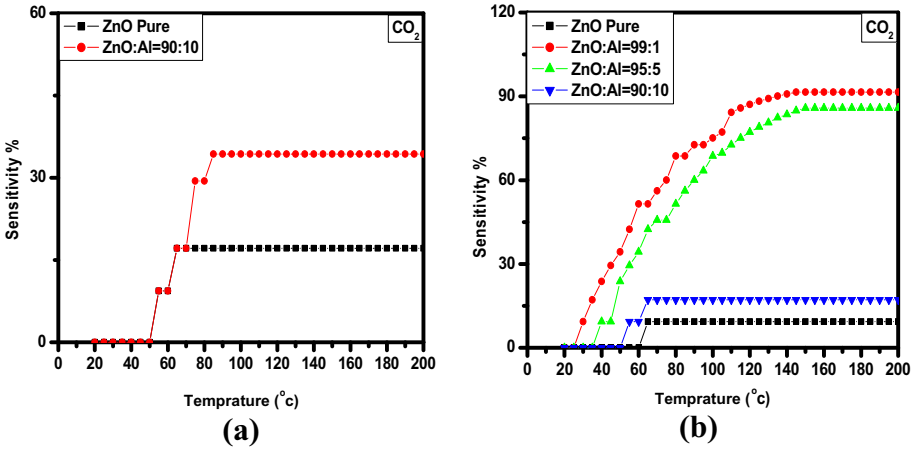

Fig. 9. Response of (a) double ZnO gas sensor, (b) quadrature pure ZnO and 1%, 5%, and 10% Al-doped ZnO gas sensors measured as a function of temperature for CO_2 gas.

O^-, the most stable form in the investigated temperature range (Eq. (6)) [33].

$$H_2 + O^-_{(ads)} \leftrightarrow H_2O + e^- \quad (6)$$

This process leads to an increase of the electron concentration, which eventually increases the conductivity of the ZnO/Al gas sensor. The sensitivity of carbon dioxide gas on the fabricated ZnO gas sensors is attributed to the chemisorption of oxygen on the sensor surface and the subsequent reaction between adsorbed oxygen anion species and the CO_2 gas. Thus, when ZnO sensor is placed in a carbon dioxide gas atmosphere, CO_2 molecules react with the pre-adsorbed oxygen species. The reaction is as follows.

$$1/2O_2 + 2e^- \Longleftrightarrow O^{2-} \quad (7)$$

$$CO_2 + O^{2-} \Longleftrightarrow CO_3^{2-} \quad (8)$$

Then the overall reaction at the sensing electrode is given by:

$$1/2O_2 + CO_2 + 2e^- \Longleftrightarrow CO_3^{2-} \quad (9)$$

As a result, the surface oxygen concentration is reduced, and electrons that were initially trapped by oxygen anions are released back into the ZnO solid, leading to an increase in the conductivity of the sensor. The reaction of CO_2 with adjacent pairs of oxygen anions produced surface bidentate carbonate species. The bidentate carbonate species subsequently transforms into surface unidentate carbonate. The adsorption of CO_2 at a single oxygen anion site then yields surface carboxylate groups. During the formation of all these surface species, there is no electron transfer to the bulk metal oxide sensor, thus no conductance change. However desorption of CO_3 provides opportunities for the electrons to return to the sensor solid. Furthermore, desorption of the formed CO_3 is favored at higher temperatures, but not favored at low temperatures [34].

For the ZnO sensors, Al doping leads to the introduction of more oxygen vacancies-related defects in ZnO nanoparticles. Therefore, more adsorption sites for gas molecules are provided by these oxygen vacancies causing the surface to become highly active for reaction [35], so that the sensing properties are improved.

4. Conclusions

The main objective of presence work was attaining ZnO gas sensor devices with high sensitivity for gas detection via double and quadrature gas sensor array. Undoped and Al-doped ZnO nanopowders with were synthesized using the sol–gel method. Structural investigations, performed by X-ray diffraction technique indicate that, studied samples are polycrystalline hexagonal wurtzite structure. Surface morphology for Undoped and Al-doped ZnO nanopowders were analyzed by scanning electron microscopy. Chemical composition of Al-doped ZnO nanopowders was performed using energy dispersive X-ray (EDS) analysis for different doping ratios. Three kinds of gases were analyzed via both double and quadrature gas sensor devices using homemade gas chamber. For oxygen gas, the best doping ratio that has a maximum oxygen sensitivity was recorded at Zn:Al = 99:1, which provided maximum sensitivity 90%. The fabricated gas sensor devices attain low carbon dioxide gas response, where the maximum CO_2 sensitivity recorded for the Al doped ZnO gas sensors with dopant ratio for ZnO:Al of 95:5 that equal 94%. The highest sensitivity values for both double and quadrature gas sensor devices established for H_2 gas. The maximum sensitivity is given at Zn:Al = 95:5 weight ratio, that get to 98%.

Conflict of interest

The authors declared no conflict of interest.

References

[1] P. Reichel, Development of a chemical gas sensor system, PhD thesis, Germany, 2005.
[2] T. Steiner, Semiconductor Nanostructures for Optoelectronic Applications, Artech House, USA, 2004. pp. 5–36.
[3] J. Arbiol, metal additive distribution in TiO_2 and SnO_2 semiconductor gas sensor nanostructured materials, PhD thesis, Barcelona, 2001.
[4] H. Chen, X. Kou, Z. Yang, W. Ni, J. Wang, Langmuir 24 (2008) 5233–5237.
[5] H.M. Chen, R.S. Liu, M.Y. Lo, S.C. Chang, L.D. Tsai, Y.M. Peng, J.F. Lee, J. Phys. Chem. C 112 (2008) 7522–7526.
[6] M. Lucas, W. Mai, R. Yang, Z.L. Wang, E. Riedo, Nano Lett. 71314-1317 (2007).
[7] Y. Qin, X.D. Wang, Z.L. Wang, Nature 45 (2008) 1809–1813.
[8] X.D. Wang, J.H. Song, J. Liu, Z.L. Wang, Science 316 (2007) 102–105.
[9] W.J.E. Beek, M.M. Wienk, R.A.J. Janssen, Adv. Mater. 16 (2004) 1009–1013.
[10] Z. Li, R.S. Yang, M. Yu, F. Bai, C. Li, Z.L. Wang, J. Phys. Chem. C 112 (2008) 20114–20117.
[11] W. Wang, B. Zeng, J. Yang, B. Poudel, J. Huang, M.J. Naughton, Z. Ren, Adv. Mater. 18 (2006) 3275–3278.
[12] Z. Yang, Y. Huang, G. Chen, Z. Guo, S. Cheng, S. Huang, Sens. Actuat. B 140 (2009) 549–556.
[13] X. Cao, W. Ning, L.D. Li, L. Guo, Sens. Actuat. B 129 (2008) 268–273.
[14] H. Gong, J.Q. Hu, J.H. Wang, C.H. Ong, F.R. Zhu, Sens. Actuat. B 115 (2006) 247–251.
[15] V.R. Shinde, T.P. Gujar, C.D. Lokhande, Sens. Actuat. B 123 (2007) 701–706.
[16] C.C. Li, L.M. Li, Z.F. Du, H.C. Yu, Y.Y. Xiang, Y. Li, Y. Cai, T.H. Wang, Nanotechnology 19 (2008) 035501.
[17] P.T. Moseley, Sens. Actuat. B 3 (1991) 167–174.
[18] C. Liewhiran, S. Phanichphant, Curr. Appl. Phys. 8 (2008) 336–339.
[19] H. Shokry Hassan, MSc thesis, Physics Department, Faculty of Science, Al-Azhar University, 2007.
[20] H. Shokry Hassan, A.B. Kashyout, H.M.A. Soliman, M.A. Uosif, N. Afify, Appl. Surface Sci. 277 (2013) 73–82.
[21] Y. Zhang, L. Liu, J. Xing, L. Yu, J. Zhang, Z. Zhang, Mater. Sci. Semiconduct. Process. 16 (2013) 1573–1579.
[22] B.L. Zhu, C.S. Xie, D.W. Zeng, W.L. Song, A.H. Wang, Mater. Chem. Phys. 89 (2005) 148–153.
[23] A.B. Kashyout, H.M.A. Soliman, H. ShokryHassan, A.M. Abousehly, J. Nanomater. 2010 (2010) (Article ID 341841).
[24] H. Nanto, T. Minami, S. Takata, J. Appl. Phys. 60 (1986) 482–484.
[25] N. Zhang, K. Yu, L. Li, Z. Zhu, Appl. Surface Sci. 254 (2008) 5736–5740.
[26] A.P. Rambu, L. Ursu, N. Iftimie, V. Nica, M. Dobromir, F. Iacomi, Appl. Surface Sci. 280 (2013) 598–604.
[27] H. Windichmann, P. Mark, J. Electrochem. Soc. 126 (1979) 627–633.
[28] C.Y. Lin, Y.Y. Fang, C.W. Lin, J.J. Tunney, K.C. Hoa, Sens. Actuat. B 146 (2010) 28–34.
[29] L.M. Li, Z.F. Du, T.H. Wang, Sens. Actuat. B 147 (2010) 165–169.
[30] D.E. Williams, Sens. Actuat. B 57 (1999) 1–16.
[31] D. Kohl, Sens. Actuat. B 18 (1989) 71–113.
[32] S. Benkara, S. Zerkout, H. Ghamri, Mater. Sci. Semiconduct. Process. 16 (2013) 1271–1279.
[33] P.G. Harrison, M.J. Willett, Nature 332 (1988) 337–339.
[34] M. Zhao, X. Wang, J. Cheng, L. Zhangc, J. Jia, X. Li, Curr. Appl. Phys. 13 (2013) 403–407.
[35] M.W. Ahn, K.S. Park, J.H. Heo, J.G. Park, D.W. Kim, K.J. Choi, J.H. Lee, S.H. Hong, Appl. Phys. Lett. 93 (2008) 263103.